SCIENTIFIC REPORTS
nature research

Corrected: Author Correction

OPEN

Anisotropic magnetocaloric effect in $Fe_{3-x}GeTe_2$

Yu Liu, Jun Li, Jing Tao, Yimei Zhu & Cedomir Petrovic

Received: 13 November 2018
Accepted: 14 August 2019
Published online: 13 September 2019

We present a comprehensive study on anisotropic magnetocaloric porperties of the van der Waals weak-itinerant ferromagnet $Fe_{3-x}GeTe_2$ that features gate-tunable room-temperature ferromagnetism in few-layer device. Intrinsic magnetocrystalline anisotropy is observed to be temperature-dependent and most likely favors the long-range magnetic order in thin $Fe_{3-x}GeTe_2$ crsytal. The magnetic entropy change ΔS_M also reveals an anisotropic characteristic between $H//ab$ and $H//c$, which could be well scaled into a universal curve. The peak value $-\Delta S_M^{max}$ of 1.20 J kg^{-1} K^{-1} and the corresponding adiabatic temperature change ΔT_{ad} of 0.66 K are deduced from heat capacity with out-of-plane field change of 5 T. By fitting of the field-dependent parameters of $-\Delta S_M^{max}$ and the relative cooling power RCP, it gives $-\Delta S_M^{max} \propto H^n$ with $n = 0.603(6)$ and $RCP \propto H^m$ with $m = 1.20(1)$ when $H//c$. Given the high and tunable T_c, $Fe_{3-x}GeTe_2$ crystals are of interest for fabricating the heterostructure-based spintronics device.

Intrinsic long-range ferromagnetism recently achieved in two-dimensional-limit van der Waals (vdW) crystals opens up great possibilities for both studying fundamental two-dimensional (2D) magnetism and engineering novel spintronic vdW heterostuctures[1–5]. Fe_3GeTe_2 is a promising candidate since its Curie temperature (T_c) in bulk is high and depends on the concentration of Fe atoms, ranging from 150 to 230 K[6–11]. Intrinsic magnetocrystalline anisotropy in few-layer counteracts thermal fluctuation and favors the 2D long-range ferromagnetism with a lower T_c of 130 K[5]. Most significantly, the T_c can be ionic-gate-tuned to room temperature in few-layers which is of high interest for electrically controlled magnetoelectronic devices[12].

The layered $Fe_{3-x}GeTe_2$ displays a hexagonal structure belonging to the $P6_3/mmc$ space group, where the 2D layers of $Fe_{3-x}Ge$ sandwiched between nets of Te ions are weakly connected by vdW bonding [Fig. 1(a)][6]. There are two inequivalent Wyckoff positions of Fe atoms which are denoted as Fe1 and Fe2. The Fe1-Fe1 dumbbells are situated in the centre of the hexagonal cell in the honeycomb lattice, composed of covalently bonded Fe2-Ge atoms. No Fe atoms occupy the interlayer space and Fe vacancies only occur in the Fe2 sites[13]. Local atomic environment is also studied by the Mössbauer and X-ray absorption spectroscopies[14,15]. Partially filled Fe d orbitals results in an itinerant ferromagnetism in $Fe_{3-x}GeTe_2$[16], which exhibits exotic physical phenomena such as nontrivial anomalous Hall effect[17–19], Kondo lattice behavior[20], strong electron correlations[21], and unusual magnetic domain structures[22,23]. A second-step satellite transition T^* is also observed just below T_c, and is not fully understood[10,15].

Here we address the anisotropy in $Fe_{3-x}GeTe_2$ as well as the magnetocaloric effect investigated by heat capacity and dc magnetization measurements. The magnetocrystalline anisotropy is observed to be temperature-dependent. The magnetic entropy change $\Delta S_M(T, H)$ also reveals an anisotropic characteristic and could be well scaled into a universal curve. Moreover, the $-\Delta S_M^{max}$ follows the power law of H^n with $n = 0.603(6)$, and the relative cooling power RCP depends on H^m with $m = 1.20(1)$.

Methods

High quality $Fe_{3-x}GeTe_2$ single crystals were synthesized by the self-flux technique[14]. The element analysis was performed using energy-dispersive X-ray spectroscopy (EDX) in a JEOL LSM-6500 scanning electron microscope (SEM). The selected area electron diffraction pattern was taken via a double aberration-corrected JEOL-ARM200F operated at 200 kV. The dc magnetization and heat capacity were measured in Quantum Design MPMS-XL5 and PPMS-9 systems with the field up to 5T.

Condensed Matter Physics and Materials Science Department, Brookhaven National Laboratory, Upton, New York, 11973, USA. Correspondence and requests for materials should be addressed to Y.L. (email: yuliu@bnl.gov) or C.P. (email: petrovic@bnl.gov)

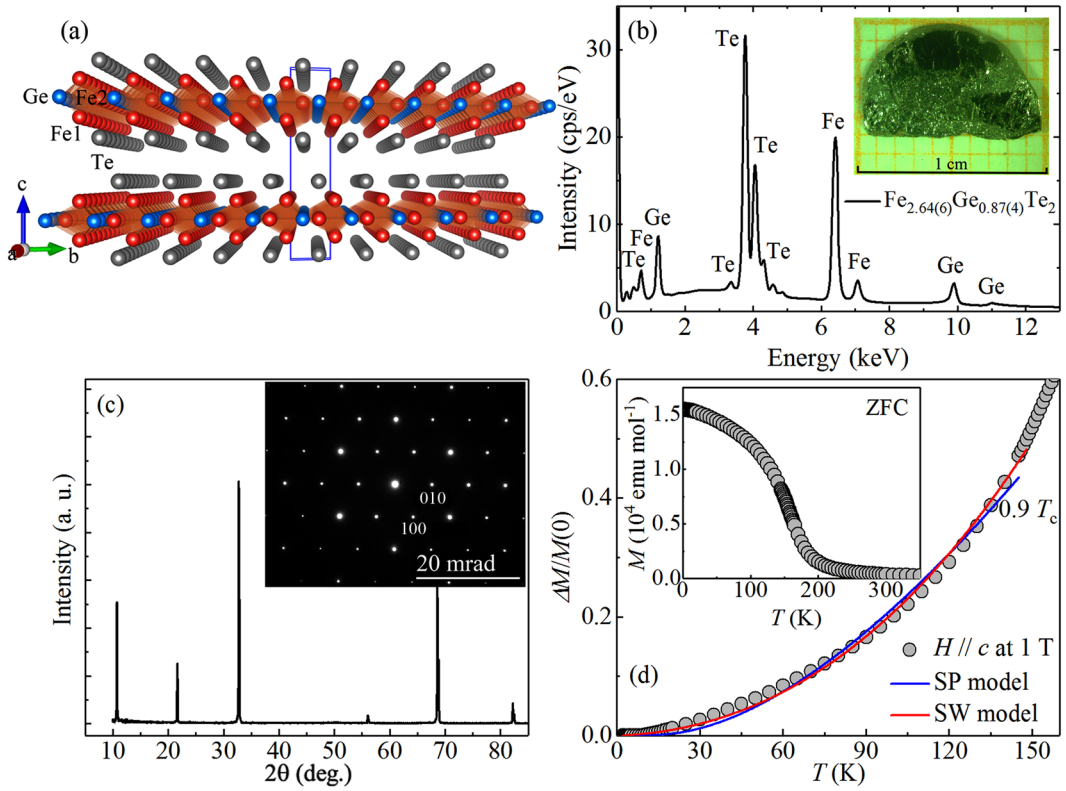

Figure 1. (**a**) Crystal structure and (**b**) X-ray energy-dispersive spectrum of $Fe_{3-x}GeTe_2$ single crystal. Inset shows a photograph of $Fe_{3-x}GeTe_2$ single crystal on a 1 mm grid. (**c**) X-ray diffraction (XRD) pattern of $Fe_{3-x}GeTe_2$. Inset shows the electron diffraction pattern taken along the [001] zone axis direction. (**d**) Temperature dependence of the reduced magnetization with out-of-plane field of $Fe_{3-x}GeTe_2$ fitted using spin-wave (SW) model and single-particle (SP) model. Inset shows the temperature dependence of zero-field-cooling (ZFC) magnetization of $Fe_{3-x}GeTe_2$ measured at $H = 1$ T applied along the c axis.

Results and Discussion

The average stoichiometry of our flux-grown $Fe_{3-x}GeTe_2$ single crystals was determined by examination of multiple points. The actual concentration is determined to be $Fe_{2.64(6)}Ge_{0.87(4)}Te_2$ [Fig. 1(b)], and it is referred to as $Fe_{3-x}GeTe_2$ throughout this paper. The as-grown single crystals are mirror-like and metallic platelets with the crystallographic c axis perpendicular to the platelet surface with dimensions up to 10 millimeters [inset in Fig. 1(b)]. In the 2θ X-ray diffraction pattern [Fig. 1(c)], only the (00l) peaks are detected, confirming the crystal surface is normal to the c axis. The corresponding electron diffraction pattern [inset in Fig. 1(c)] also confirms the high quality of single crystals.

Figure 1(d) presents the low temperature thermal demagnetization analysis for $Fe_{3-x}GeTe_2$ with out-of-plane field using both spin-wave (SW) model and single-particle (SP) model. The temperature dependence of zero-field-cooling (ZFC) magnetization $M(T)$ for $Fe_{3-x}GeTe_2$ measured in $H = 1$ T applied along the c axis is shown in the inset of Fig. 1(d). Localized-moment spin-wave excitations can be described by a Bloch equation[24–26]:

$$\frac{\Delta M}{M(0)} = \frac{M(0) - M(T)}{M(0)} = AT^{3/2} + BT^{5/2} + \cdots, \quad (1)$$

where A and B are the coefficients. The $M(0)$ is the magnetization at 0 K, which is usually estimated from the extrapolation of $M(T)$. The $T^{3/2}$ term stems from harmonic contribution and the $T^{5/2}$ term is a high-order contribution in spin-wave dispersion relation. In an itinerant magnetism, it is a result of excitation of electrons from one subband to the other. The single-particle excitation is[24]:

$$\frac{\Delta M}{M(0)} = \frac{M(0) - M(T)}{M(0)} = CT^{3/2} exp\frac{-\Delta}{k_B T}, \quad (2)$$

where C, Δ and k_B are fit coefficient, the energy gap between the Fermi level and the top of the full subband and the Boltzmann constant, respectively. It can be seen that the SW model gives a better fit than the SP model up to 0.9 T_c [Fig. 1(d)], indicating possible localized moment, in agreement with the bad-metallic resistivity of $Fe_{3-x}GeTe_2$[15]. It is also understandable that the SP model fails due to strong electron correlation in $Fe_{3-x}GeTe_2$[21]. The fitting yields $A = 8.4(7) \times 10^{-5}$ K$^{-3/2}$, $B = 1.24(5) \times 10^{-6}$ K$^{-5/2}$, $C = 3.4(1) \times 10^{-4}$ K$^{-3/2}$ and $\Delta = 3.9(4)$ meV.

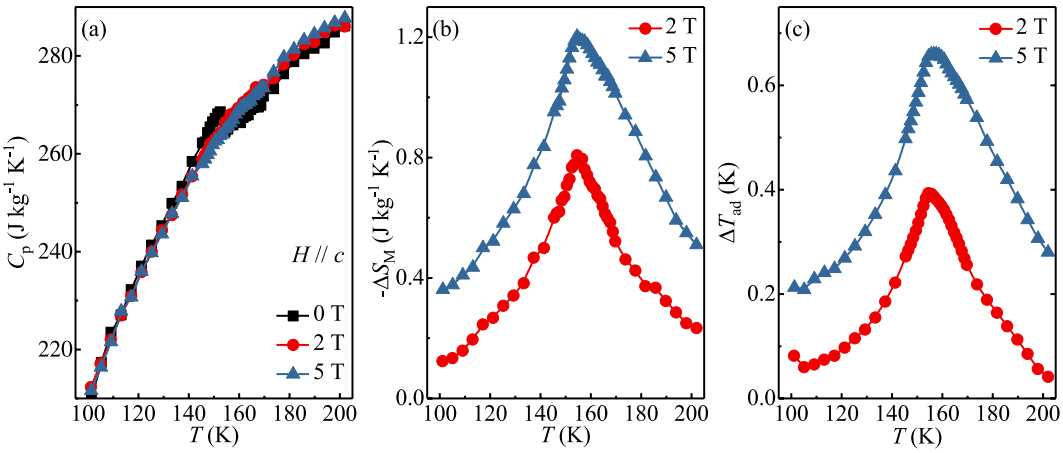

Figure 2. Temperature dependences of (**a**) the specific heat C_p, (**b**) the magnetic entropy change $-\Delta S_M$, and (**c**) the adiabatic temperature change ΔT_{ad} for $Fe_{3-x}GeTe_2$ with out-of-plane field changes of 2 and 5T.

Figure 2(a) shows the temperature dependence of heat capacity C_p for $Fe_{3-x}GeTe_2$ measured in zero-field and out-of-plane field of 2 and 5 T, respectively. The ferromagnetic order anomaly at $T_c = 153$ K in the absence of magnetic field is gradually suppressed in fields. The entropy $S(T, H)$ can be determined by

$$S(T, H) = \int_0^T \frac{C_p(T, H)}{T} dT. \tag{3}$$

The magnetic entropy change $\Delta S_M(T, H)$ can be approximated as $\Delta S_M(T, H) = S_M(T, H) - S_M(T, 0)$. In addition, the adiabatic temperature change ΔT_{ad} caused by the field change can be derived by $\Delta T_{ad}(T, H) = T(S, H) - T(S, 0)$ at constant total entropy $S(T, H)$. Figure 2(b,c) present the temperature dependence of $-\Delta S_M$ and ΔT_{ad} estimated from heat capacity with out-of-plane field. They are asymmetric and attain a peak around T_c. The maxima of $-\Delta S_M$ and ΔT_{ad} increase with increasing field and reach the values of 1.20 J kg^{-1} K^{-1} and 0.66 K, respectively, with the field change of 5 T. Since a large magnetic anisotropy is observed in $Fe_{3-x}GeTe_2$, it is of interest to further calculate its anisotropic magnetic entropy change.

Figure 3(a,b) present the magnetization isotherms with field up to 5 T applied in the *ab* plane and along the *c* axis, respectively, in temperature range from 100 to 200 K with a temperature step of 4 K. The magnetic entropy change can be obtained from dc magnetization measurement as[27]:

$$\Delta S_M(T, H) = \int_0^H \left[\frac{\partial S(T, H)}{\partial H}\right]_T dH. \tag{4}$$

With the Maxwell's relation $\left[\frac{\partial S(T,H)}{\partial H}\right]_T = \left[\frac{\partial M(T,H)}{\partial T}\right]_H$, it can be rewritten as[28]:

$$\Delta S_M(T, H) = \int_0^H \left[\frac{\partial M(T, H)}{\partial T}\right]_H dH. \tag{5}$$

When the magnetization is measured at small temperature and field steps, $\Delta S_M(T, H)$ is approximated:

$$\Delta S_M(T, H) = \frac{\int_0^H M(T + \Delta T) dH - \int_0^H M(T) dH}{\Delta T}. \tag{6}$$

Figure 3(c,d) show the calculated $-\Delta S_M(T, H)$ as a function of temperature in various fields up to 5 T applied in the *ab* plane and along the *c* axis, respectively. All the $-\Delta S_M(T, H)$ curves feature a pronounced peak around T_c, similar to those obtained from heat capacity [Fig. 2(b)], and the peak broadens asymmetrically on both sides with increase in field. Moreover, the value of $-\Delta S_M(T, H)$ increases monotonically with increase in field; the peak $-\Delta S_M$ reaches 1.26 J kg^{-1} K^{-1} with in-plane field change and 1.44 J kg^{-1} K^{-1} with out-of-plane change of 5 T, respectively. We calculated the rotating magnetic entropy change ΔS_M^R as

$$\Delta S_M^R(T, H) = \Delta S_M(T, H_c) - \Delta S_M(T, H_{ab}). \tag{7}$$

The asymmetry of $-\Delta S_M(T, H)$ is more apparent in the temperature dependence of $-\Delta S_M^R$ [Fig. 3(e)]. Furthermore, there is a slight shift of $-\Delta S_M$ maximum towards higher temperature when the field varies from 1 to 5 T [Fig. 3(c,d)]. This shift of T_{peak} excludes the mean field model but could be reproduced by the Heisenberg model due to its discrepancy with T_c[29].

Around the second order phase transition[30], the magnetic entropy maximum change is $-\Delta S_M^{max} = aH^n$ [31], where a is a constant and n is[32]

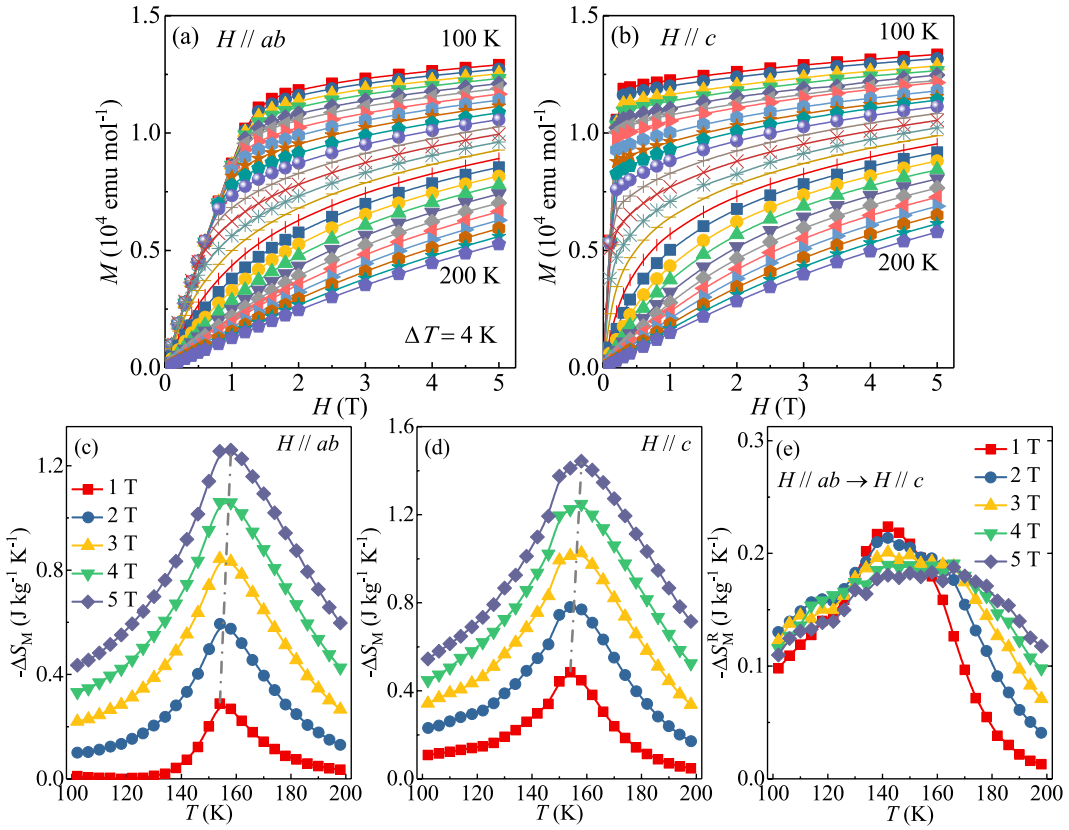

Figure 3. Initial isothermal magnetization curves from $T = 100$ to 200 K with temperature step of $T = 4$ K measured with (**a**) in-plane and (**b**) out-of-plane fields. Temperature dependence of magnetic entropy change $-\Delta S_M$ obtained with (**c**) in-plane and (**d**) out-of-plane field changes, and (**e**) the difference $-\Delta S_M^R$.

$$n(T, H) = dln|\Delta S_M|/dln(H). \tag{8}$$

Figure 4(a) shows the temperature dependence of $n(T)$ in various fields. All the $n(T)$ curves follow an universal behavior[33]. At low temperatures, n has a value close to 1. At high temperatures, n tends to 2 as a consequence of the Curie-Weiss law. At $T = T_c$, n has a minimum. Additionally, the exponent n at T_c is related to the critical exponents[30]:

$$n(T_c) = 1 + \left(\frac{\beta - 1}{\beta + \gamma}\right) = 1 + \frac{1}{\delta}\left(1 - \frac{1}{\beta}\right), \tag{9}$$

where β, γ, and δ are the critical exponents related to the spontaneous magnetization M_s below T_c, the inverse initial susceptibility H/M above T_c, and the isotherm $M(H)$ at T_c, respectively.

Relative cooling power (RCP) could be used to estimate the cooling efficiency[34]:

$$RCP = -\Delta S_M^{max} \times \delta T_{FWHM}, \tag{10}$$

where $-\Delta S_M^{max}$ is the entropy change maximum around T_c and δT_{FWHM} is the width at half maximum. The RCP also depends on the field as $RCP = bH^m$, where b is a constant and m is related to the critical exponent δ:

$$m = 1 + \frac{1}{\delta}. \tag{11}$$

Figure 4(b) presents the field-dependent $-\Delta S_M^{max}$ and RCP. The RCP is 113.3 J kg^{-1} within field change of 5 T for $Fe_{3-x}GeTe_2$. This is one half of those in manganites and much lower than in ferrites[35,36]. Fitting of the $-\Delta S_M^{max}$ and RCP gives $n = 0.603(6)$ and $m = 1.20(1)$, which are close to the values estimated from the critical exponents (Table 1).

The scaling of magnetocaloric data is constructed by normalizing all the $-\Delta S_M$ curves against the maximum $-\Delta S_M^{max}$, namely, $\Delta S_M/\Delta S_M^{max}$ by rescaling the temperature t below and above T_c as defined in:

$$t_- = (T_{peak} - T)/(T_{r1} - T_{peak}),\ T < T_{peak}, \tag{12}$$

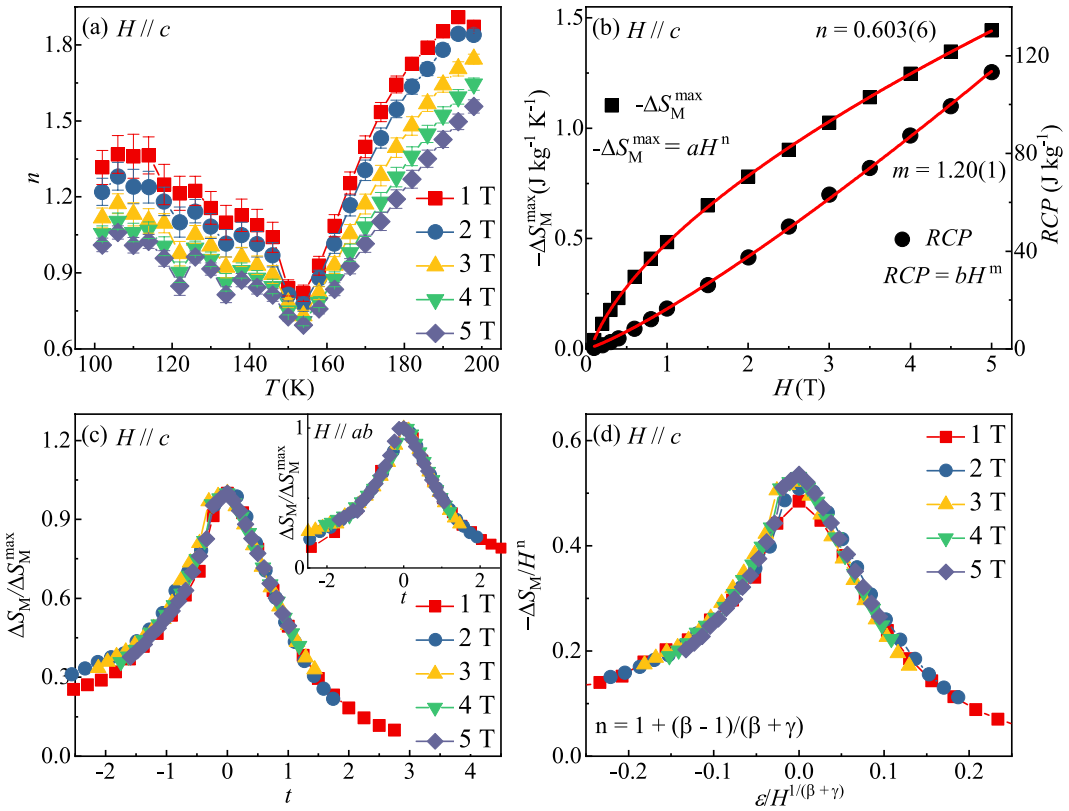

Figure 4. (**a**) Temperature dependence of n in various fields. (**b**) Field dependence of the maximum magnetic entropy change $-\Delta S_M^{max}$ and the relative cooling power RCP with power law fitting in red solid lines. (**c**) The normalized ΔS_M as a function of the rescaled temperature t with out-of-plane field and in-plane field (inset). (**d**) Scaling plot based on the critical exponents $\beta = 0.372$ and $\gamma = 1.265$[14].

Technique	β	γ	δ	n	m
$-\Delta S_M^{max}$				0.603(6)	
RCP					1.20(1)
MAP	0.374(1)	1.273(8)	4.404(12)	0.620(1)	1.227(1)
KFP	0.372(4)	1.265(15)	4.401(6)	0.616(2)	1.227(1)
CI			4.50(1)		1.222(1)

Table 1. Critical exponents of $Fe_{3-x}GeTe_2$[14]. The MAP, KFP and CI represent the modified Arrott plot, the Kouvel-Fisher plot and the critical isotherm, respectively.

$$t_+ = (T - T_{peak})/(T_{r2} - T_{peak}),\ T > T_{peak}, \tag{13}$$

where T_{r1} and T_{r2} are the temperatures of two reference points corresponding to $\Delta S_M(T_{r1}, T_{r2}) = \frac{1}{2}\Delta S_M^{max}$[37]. All the $-\Delta S_M(T, H)$ curves collapse onto a single curve regardless of temperature and field, as shown in Fig. 4(c). In the phase transition region, the scaling analysis of $-\Delta S_M$ can also be expressed as

$$\frac{-\Delta S_M}{a_M} = H^n f\left(\frac{\varepsilon}{H^{1/\Delta}}\right), \tag{14}$$

where $a_M = T_c^{-1}A^{\delta+1}B$ with A and B representing the critical amplitudes as in $M_s(T) = A(-\varepsilon)^\beta$ and $H = BM^\delta$, $\Delta = \beta + \gamma$, and $f(x)$ is the scaling function[38]. If the critical exponents are appropriately chosen, the $-\Delta S_M(T)$ curves should be rescaled into a single curve, consistent with normalizing all the $-\Delta S_M$ curves with two reference temperatures. By using the values of $\beta = 0.372$ and $\gamma = 1.265$ obtained by the Kouvel-Fisher plot[14], we have replotted the scaled $-\Delta S_M$ for $Fe_{3-x}GeTe_2$ [Fig. 4(d)]. The good overlap of the experimental data points clearly indicates that the obtained critical exponents for $Fe_{3-x}GeTe_2$ are not only in agreement with the scaling hypothesis but also intrinsic.

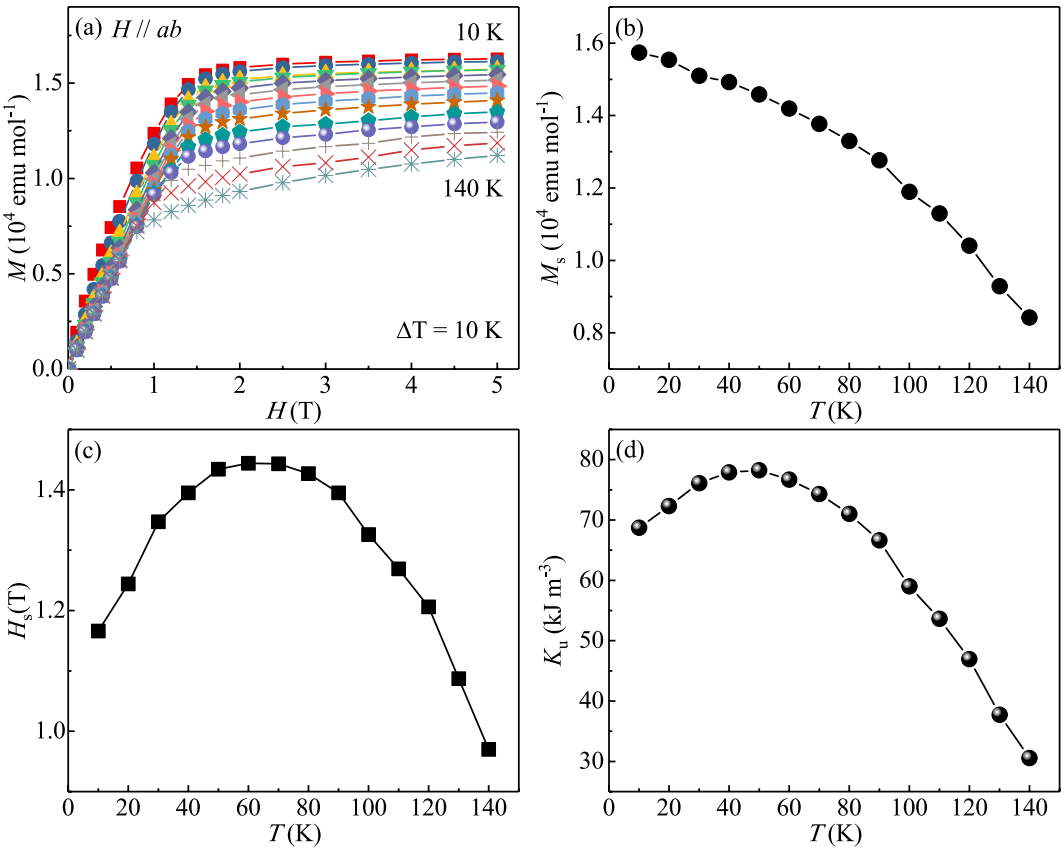

Figure 5. (**a**) Initial isothermal magnetization curves from $T = 10$ to 140 K with in-plane fields. Temperature evolution of (**b**) the saturation magnetization M_s, (**c**) the saturation field H_s, and (**d**) the anisotropy constant K_u.

Then we estimated the magnetocrystalline anisotropy of $Fe_{3-x}GeTe_2$. By using the Stoner-Wolfarth model a value for the magnetocrystalline anisotropy constant K_u can be estimated from the saturation regime in isothermal magnetization curves [Fig. 5(a)][39]. Within this model the magnetocrystalline anisotropy in the single domain state is related to the saturation magnetic field H_s and the saturation moment M_s with μ_0 is the vacuum permeability:

$$\frac{2K_u}{M_s} = \mu_0 H_{sat}. \tag{15}$$

When $H//ab$, the anisotropy becomes maximal. We estimated the saturation magnetization M_s by using a linear fit of $M(H)$ above a magnetic field of 2.5 T with in-plane field [Fig. 5(b)], which monotonically decreases with increasing temperature. Then we determined the saturation field H_s as the intersection point of two-linear fits, one being a fit to the saturated regime at high fields and one being a fit of the unsaturated linear regime at low fields. The value of H_s increases at low temperature, which is possibly related to a spin reorientation transition[15], and then decreases with increasing temperature [Fig. 5(c)]. Figure 5(d) presents the temperature evolution of K_u for $Fe_{3-x}GeTe_2$, which can not be described by the $l(l+1)/2$ power law[40,41]. The value of K_u for $Fe_{3-x}GeTe_2$ is about 69 kJ cm^{-3} at 10 K, slightly increases to 78 kJ cm^{-3} at 50 K, and then decrease with increasing temperature, which are comparable to those for $CrBr_3$, but smaller than those for CrI_3[42]. The decrease of K_u with increasing temperature is also observed in $CrBr_3$ and CrI_3[42], arising from a large number of local spin clusters[43,44]. In a pure two-dimensional system, materials with isotropic short-range exchange interactions can not magnetically order. The long-range ferromagnetism in few-layers of $Fe_{3-x}GeTe_2$ could possibly be favored by the large magnetocrystalline anisotropy.

Conclusion

In summary, we have investigated in detail the magnetocaloric effect of $Fe_{3-x}GeTe_2$ single crystals. The large magnetocrystalline anisotropy is found to be temperature-dependent and probably establishes the long-range ferromagnetism in few-layers of $Fe_{3-x}GeTe_2$. The magnetic entropy change $-\Delta S_M$ also reveals an anisotropic characteristic and could be well scaled into a universal curve independent on temperature and field. By fitting of the field-dependent parameters of $-\Delta S_M^{max}$ and the relative cooling power RCP, it gives $-\Delta S_M^{max} \propto H^n$ with $n = 0.603(6)$ and $RCP \propto H^m$ with $m = 1.20(1)$ when $H//c$. Considering its tunable room-temperature ferromagnetism and hard magnetic properties in nanoflakes, further investigation on the size dependence of magnetocaloric effect is of interest.

References

1. McGuire, M. A. *et al*. Coupling of Crystal Structure and Magnetism in the Layered, Ferromagnetic Insulator CrI_3. *Chem. Mater.* **27**, 612 (2015).
2. Huang, B. *et al*. Layer-dependent ferromagnetism in a van der Waals crystal down to the monolayer limit. *Nature* **546**, 270 (2017).
3. Gong, C. *et al*. Discovery of intrinsic ferromagnetism in two-dimensional van der Waals crystals. *Nature* **546**, 265 (2017).
4. Seyler, K. L. *et al*. Ligand-field helical luminescence in a 2D ferromagnetic insulator. *Nature Physics* **14**, 277 (2018).
5. Fei, Z. *et al*. Two-dimensional itinerant ferromagnetism in atomically thin Fe_3GeTe_2. *Nature Materials* **17**, 778 (2018).
6. Deiseroth, H. J. *et al*. Fe_3GeTe_2 and Ni_3GeTe_2 — Two New Layered Transition Metal Compounds: Crystal Structures, HRTEM Investigations, and Magnetic and Electrical Properties. *Eur. J. Inorg. Chem.* **2006**, 1561 (2006).
7. Chen, B. *et al*. Magnetic Properties of Layered Itinerant Electron Ferromagnet Fe_3GeTe_2. *J. Phys. Soc. Jpn.* **82**, 124711 (2013).
8. May, A. F. *et al*. Magnetic structure and phase stability of the van der Waals bonded ferromagnet $Fe_{3-x}GeTe_2$. *Phys. Rev. B* **93**, 014411 (2016).
9. Liu, S. *et al*. Wafer-scale two-dimensional ferromagnetic Fe_3GeTe_2 thin films grown by molecular beam epitaxy. *npj 2D Mater. Appl.* **1**, 30 (2017).
10. Yi, J. Y. *et al*. Competing antiferromagnetism in a quasi-2D itinerant ferromagnet: Fe_3GeTe_2. *2D Mater.* **4**, 011005 (2016).
11. Liu, B. *et al*. Critical behavior of the van der Waals bonded high T_c ferromagnet Fe_3GeTe_2. *Sci. Rep.* **7**, 6184 (2017).
12. Deng, Y. *et al*. Gate-tunable room-temperature ferromagnetism in two-dimensional Fe_3GeTe_2. *Nature* **563**, 94 (2018).
13. Verchenko, V. Y. *et al*. Ferromagnetic Order, Strong Magnetocrystalline Anisotropy, and Magnetocaloric Effect in the Layered Telluride $Fe_{3-x}GeTe_2$. *Inorg. Chem.* **54**, 8598 (2015).
14. Liu, Y., Ivanovski, V. N. & Petrovic, C. Critical behavior of the van der Waals bonded ferromagnet $Fe_{3-x}GeTe_2$. *Phys. Rev. B* **96**, 144429 (2017).
15. Liu, Y., Stavitski, E. & Attenkofer, K. & Petrovic, C. Anomalous Hall effect in the van der Waals bonded ferromagnet $Fe_{3-x}GeTe_2$. *Phys. Rev. B* **97**, 165415 (2018).
16. Zhuang, H. L. *et al*. Strong anisotropy and magnetostriction in the two-dimensional Stoner ferromagnet Fe_3GeTe_2. *Phys. Rev. B* **93**, 134407 (2016).
17. Kim, K. *et al*. Large anomalous Hall current induced by topological nodal lines in a ferromagnetic van der Waals semimetal. *Nat. Mater.* **17**, 794 (2018).
18. Wang, Y. *et al*. Anisotropic anomalous Hall effect in triangular itinerant ferromagnet Fe_3GeTe_2. *Phys. Rev. B* **96**, 134428 (2017).
19. Tan, C. Hard magnetic properties in nanoflake van der Waals Fe_3GeTe_2. *Nat. Commun.* **9**, 1554 (2018).
20. Zhang, Y. *et al*. Emergence of Kondo lattice behavior in a van der Waals itinerant ferromagnet, Fe_3GeTe_2. *Sci. Adv.* **4**, eaao6791 (2018).
21. Zhu, J. X. *et al*. Electronic correlation and magnetism in the ferromagnetic metal Fe_3GeTe_2. *Rhys. Rev. B* **93**, 144404 (2016).
22. Nguyen, G. *et al*. Visualization and manipulation of magnetic domains in the quasi-two-dimensional material Fe_3GeTe_2. *Rhys. Rev. B* **97**, 014425 (2018).
23. León-Brito, N. *et al*. Magnetic microstructure and magnetic properties of uniaxial itinerant ferromagnet Fe_3GeTe_2. *J. Appl. Phys.* **120**, 083903 (2016).
24. Das, A. & Majumdar, A. K. Magnetic properties of Co-rich amorphous alloys containing Cr/Mn. *J. Magn. Magn. Mater.* **128**, 47 (1993).
25. Kaul, S. N. Low-temperature magnetization and spin-wave excitations in amorphous Ni-rich transition-metal—metalloid alloys. *Phys. Rev. B* **27**, 5761 (1983).
26. Kaul, S. N. Spin-wave, Stoner single-particle and correlated particle-hole pair contributions to thermal demagnetization in amorphous $Fe_{90+x}Zr_{10-x}$. *J. Phys.: Condens. Matter* **3**, 4027 (1991).
27. Pecharsky, V. & Gscheidner, K. Magnetocaloric effect and magnetic refrigeration. *J. Magn. Magn. Mater.* **200**, 44 (1999).
28. Amaral, J. *et al*. Magnetocaloric effect in Er-and Eu-substituted ferromagnetic La-Sr manganites. *J. Magn. Magn. Mater.* **290**, 686 (2005).
29. Franco, V. *et al*. The magnetocaloric effect in materials with a second order phase transition: Are T_c and T_{peak} necessarily coincident. *J. Appl. Phys.* **105**, 07A917 (2009).
30. Oesterreicher, H. & Parker, F. T. Magnetic cooling near Curie temperatures above 300 K. *J. Appl. Phys.* **55**, 4334 (1984).
31. Franco, V. *et al*. Field dependence of the magnetocaloric effect in materials with a second order phase transition: A master curve for the magnetic entropy change. *Appl. Phys. Lett.* **89**, 222512 (2006).
32. Franco, V. *et al*. Field dependence of the magnetocaloric effect in core-shell nanoparticles. *J. Appl. Phys.* **107**, 09A902 (2010).
33. Franco, V. *et al*. The influence of a minority magnetic phase on the field dependence of the magnetocaloric effect. *J. Magn. Magn. Mater.* **321**, 1115 (2009).
34. Gschneidner, K. A. Jr. *et al*. Recent Developments in Magnetic Refrigeration. *Mater. Sci. Forum* **315–317**, 69 (1999).
35. Phan, M. H. & Yu, S. C. Review of the magnetocaloric effect in manganite materials. *J. Magn. Magn. Mater.* **308**, 325 (2007).
36. Maalam, K. E. *et al*. Magnetocaloric Properties of Zinc-Nickel Ferrites Around Room Temperature. *J. Supercond. Nov. Magn.* **30**, 1943 (2017).
37. Franco, V. & Conde, A. Scaling laws for the magnetocaloric effect in second order phase transitions: From physics to applications for the characterization of materials. *Int. J. Refrig.* **33**, 465 (2010).
38. Su, Y. *et al*. Critical behavior of the ferromagnetic perovskites $RTiO_3$ (R = Dy, Ho, Er, Tm, Yb) by magnetocaloric measurements. *Phys. Rev. B* **87**, 195102 (2013).
39. Stoner, E. C. & Wohlfarth, E. P. A mechanism of magnetic hysteresis in heterogeneous alloys. *Philos. Trans. R. Soc. Lond. Ser. Math. Phys. Sci.* **240**, 599 (1948).
40. Callen, H. B. & Callen, E. The present status of the temperature dependence of magnetocrystalline anisotropy, and the $l(l+1)/2$ power law. *J. Phys. Chem. Solids.* **27**, 1271 (1966).
41. Mryasov, O. N. *et al*. Temperature-dependent magnetic properties of FePt: Effect spin Hamiltonian model. *Europhys. Lett.* **69**, 805 (2005).
42. Richter, N. *et al*. Temperature-dependent magnetic anisotropy in the layered magnetic semiconductors CrI_3 and $CrBr_3$. *Phys. Rev. Mater.* **2**, 024004 (2018).
43. Zener, C. Classical Theory of the Temperature Dependence of Magnetic Anisotropy Energy. *Phys. Rev.* **96**, 1335 (1954).
44. Carr, W. J. Temperature Dependence of Ferromagnetic Anisotropy. *J. Appl. Phys.* **29**, 436 (1958).

Acknowledgements

We thank J. Warren for help with the scanning electron microscopy (SEM) measurement. Work at Brookhaven National Laboratory was supported by US DOE, Office of Science, Office of Basic Energy Sciences under contract DE-SC0012704.

Author Contributions

Y.L. and C.P. designed this study and synthesized crystals; Y. L. performed magnetization and heat capacity measurements. J.L., J.T. and Y.Z. contributed TEM measurement. Y.L. and C.P. organized and wrote the paper with input from all collaborators. This manuscript reflects the contribution and ideas of all authors.

Additional Information

Competing Interests: The authors declare no competing interests.

Publisher's note: Springer Nature remains neutral with regard to jurisdictional claims in published maps and institutional affiliations.